Supporting Information

Both sides matter: Anode Configurations alter the Activity of Electrolyzers for Organic Hydrogenation

Kevinjeorjios Pellumbi†[a,b], Jonas Wolf†[a,b], Sangita Viswanathan[A,b], Leon Wickert[a,b], Mena-Alexander Kräenbring[c], Julian T. Kleinhaus[b], Kai junge Puring[a], Fatih Özcan[3], Doris Segets[c,d], Ulf-Peter Apfel[a,b] and Daniel Siegmund[a,b]**

[a] *Fraunhofer Institute for Environmental, Safety and Energy Technology, UMSICHT, Oberhausen, Germany*

[b] *Inorganic Chemistry, Faculty of Chemistry and Biochemistry, Ruhr-University Bochum, Bochum, Germany*

[c] *Institute for Energy and Materials Processes – Particle Science and Technology (EMPI-PST), Duisburg, Germany*

[d] *Center for Nanointegration Duisburg-Essen (CENIDE), University of Duisburg-Essen, Duisburg, Germany*

**Correspondence: ulf.apfel@umsicht.fraunhofer.de, ulf.apfel@rub.de and daniel.siegmund@umsicht.fraunhofer.de*

† *These authors contributed equally*

Table of contents

Materials

Unless otherwise stated, all chemicals were purchased from commercial vendors and used without further purification. The elemental iron, nickel, and sulphur used for the synthesis of the different pentlandites were purchased from Alfa Aesar. 2-methyl-3-butyn-2-ol (98 %), 2-methyl-3-buten-2-ol, (98 %) and 2-methyl-3-butan-2-ol (98 %) were purchased from Sigma Aldrich. The Fumasep FAA-3-PK-130 and the Nafion 115, ion-exchange membranes were purchased by Quitech Gmbh, while IrO_2 (Iridium(IV)-oxide, Premion™, 99.99 % (Metallbasis), Ir 84.5 % min.) was purchased by Fischer Scientific. The porous transport layers (PTLs) used in this work were bought by the following commercial vendors: H23 carbon paper (Quintech GmbH), SGL-GFD-2.5 mm (Sigracell), Stainless Steel Mesh (Haver-Boecker), Titanium PTLs (2-GDL40, Bekaert) and used without further modifications.

Mechanochemical synthesis of the used $Fe_3Ni_6S_8$ catalyst

The synthesis of the $Fe_3Ni_6S_8$ pentlandite catalyst was conducted through mechanochemical means, as previously reported.[1] Under argon atmosphere, 5 g of a stoichiometric mixture of the elemental powders and 24 g of 2 mm zirconium oxide milling balls were mixed in a 20 mL zirconium oxide grinding vessel. In a Fritsch Planetary Micro Mill Pulverisette 7 premium line, the mixture was milled for 120 min at 1100 rpm for two cycles with a 60 min break in between to obtain the pentlandite catalyst.

Electrode fabrication

To prepare the cathode, we employed our previously reported PTFE-containing catalytic inks.[2] In short, 0.5 g of the mechanochemically synthesized $Fe_3Ni_6S_8$ catalyst was mixed with 15 g 2-propanol, 4 mL H_2O, and 0.2 g Triton X 100. The mixture was placed into an ultrasonic bath for 5 min. Afterwards, the ink was dispersed at 13,600 rpm using a T 25 digital Ultra-Turrax for 1 min. Afterwards, the respective amount of a 60 wt.% PTFE dispersion was added while stirring. The suspension was then homogenously spray-coated with an Iwata SBS airbrush on an 8.5x8.5 cm carbon cloth or carbon felt that was heated on a hot plate to 100 °C. Afterwards, the PTFE-containing electrodes were heat-treated at 240 °C for 20 min to remove the added surfactants.

For the anode fabrication, 500 mg of IrO_2 (Thermofischer) was

The resulting catalyst-coated sheets were cut into circular electrodes of a diameter of 40 mm with the help of an iron punch. The catalytic loading was determined through the weight difference between the non-coated substrates and the coated electrodes after drying.

Hot-pressing of the CCM-prepared membranes on the different anode PTLs was performed at 120 °C at 10 bar for 30 seconds.

Electrochemical investigations in a zero-gap electrolyzer

The electrochemical investigations in membrane electrode assemblies (MEAs) were performed in an in-house built single-cell electrolyzer with an electrode area of 12.57 cm^2 (40 mm diameter). A compressed Ni-foam served as the anode and a porous carbon electrode coated with 5 mg cm^{-2} of the respective catalysts served as the cathode. PTFE gaskets and a torque value of 5 N m over eight screws were employed to ensure a leak-less operation. The used Fumasep membranes were conditioned overnight in 1 M KOH before use. During electrolysis, the anolyte and catholyte solutions were circulated through the half-cells at a flow rate of 12 ml min^{-1}, while a homogeneous liquid distribution was guaranteed with Ti-based serpentine flow fields. A copper plate in direct contact with the flow field served as the current collector plate. Electrolysis was performed for 2 h, with samples being taken at the end of the electrolysis from both the anolyte and the catholyte. The respective chronopotentiometric curves up to a current density of 80 mA cm^{-2} (1 A) were recorded on a Gamry Interface 1010B potentiostate/galvanostate, while for current density values above 80 mA cm^{-2}, a Gamry Reference 3000 potentiostate/galvanostate was employed. For each experiment, a new MEA was constructed/investigated, with each experiment being repeated at least twice to ensure reproducibility.

EIS analysis was performed potentiostatically at a cell voltage of 2.9 V, between 1 Hz –100 Hz with a 10 mV rms perturbartion. Control of the EIS data was performed via the Kramers-Kroning test.

Nuclear Magnetic Resonance (NMR) analysis

The catholyte and anolyte solution samples were additionally analyzed via ^{1}H-NMR spectroscopy with potassium hydrogen phthalate as the internal standard. NMR samples consisted of 50 µl sample solution, 50 µl of a solution containing 1.25 µmol potassium hydrogen phthalate standard in D_2O and 400 µl D_2O as solvent. ^{1}H-NMR analysis was conducted using an Avance-III 300 MHz spectrometer at 22 °C. Under the applied conditions and concentrations, equal integrals of the standard and the product protons correspond to equal concentrations. This was confirmed by control experiments with known amounts of MBY, MBE, and MBA.

Product quantification for the zero-gap experiments

The faradaic efficiency (FE) of MBE and MBA was calculated with equation 1, (with n_p as the amount of product p in mol, z as the number of transferred electrons (z = 2 for MBE, z = 4 for MBA), F as Faraday constant (96485 A s mol^{-1}), I as applied absolute current in A and t as reaction time (7200 s)):

$$F.E._p = n_p \cdot \frac{zF}{I \cdot t} \cdot 100\ \% \tag{1}$$

The amount of product n_p was calculated with equation 2 (with I as the integral of the product peak (6H) in the ^{1}H-NMR spectrum normalized to the peak integral of the internal standard (4H), and n_{St} as the amount of internal standard in the NMR sample (1.25 µmol)):

$$n_p = I \cdot {}^2/_3 \cdot n_{St} \cdot 1000 \tag{2}$$

The yield was determined with equation 3:

$$yield = \frac{n_p}{n_{MBY}} \cdot 100\ \% \tag{3}$$

FE and yield error bars were calculated from the results of duplicates.

The potential values have been calculated by determining the arithmetic mean of the respective potential data for all data points of the last 10 min of the experiment for both of the two measurements. The arithmetic mean and the standard deviation of the resulting values were determined as the final data points of the respective experiment.

For the quantification of hydrogen, the zero-gap electrolyzers under investigation were coupled to an online Shimdazu QP2020 GC-MS equipped with a Supelco Carboxen 1010 Plot column. The catholyte reservoir was completely sealed with Ar flowing through at a flow rate of 10 ml min^{-1} at an overpressure of 50 mbar in the catholyte compartment. Gas-samples were taken every 1 h for a total of 10 h, at 80 mA cm^{-2}.

Atomic force microscopy (AFM) analysis

The atomic force microscopy (AFM) measurements were conducted using an Anton Paar Tosca 400 atomic force microscope. Each sample was cut into a 1 cm^2 square and glued to the sample holder using a double-sided copper tape. The measurements were carried out using a contact mode tip, a scanning area of 10 µm by 10 µm and a scan rate of 0.1 lines per second. The resulting image was then analyzed using the Tosca Analysis software (Version 7.4.9286). The topography data was leveled and any measurement artefacts were digitally touched up. The surface roughness values were calculated according to the arithmetical mean height as defined in ISO 25178 in the final step.

Visualization of the compression pressure

A Prescale film from Fujifilm was employed to measure and visualize the pressure distribution within the MEA. The low-pressure (LW) film set was inserted between the cathode and anode porous-transport layers (PTLs) instead of the membrane and the eight screws were tightened with a torque of 5 N m. After allowing the dye reaction to proceed for 2 min, analysis of the pressure distribution was performed with the accompanying Epson Perfection Scanner via the help of the FDF-808E software. Prior to each measurement cycle, software calibration was performed with the help of the included calibration sheet.

Detailed description of the tested cell assemblies

Table S1. Tabular description of all experiments performed in our zero-gap electrolyzer for the different cell assemblies, aiming to further aid researchers of understanding/selecting specific trends.

Anode PTL	Cathode PTL	Membrane Type	Deposition Type	FE_{MBE}	FE_{MBA}	U_{cell}
Ti-1 mm	H23	AEM	CCM	41.4±1.2	13.3±5.2	2.9±0.01
Ti-0.15 mm	H23	AEM	CCM	38.3±4.4	2±0.2	2.9±0.04
Ti-1 mm	SGL	AEM	CCM	41.4±3.8	8.3±2.7	3.2±0.006
Ti-0.15 mm	SGL	AEM	CCM	45.8±3.5	7.5±1.2	3.2±0.01
SSM	SGL	AEM	CCM	36.8±9.6	10.2±3.0	3.3±0.06
H23	SGL	AEM	CCM	43.1±7.6	10.1±0.7	3.9±0.06
Ti-1 mm	H23	AEM	CCS	35.6±2.5	12.4±1.8	3.7±0.01
Ti-0.15 mm	H23	AEM	CCS	43.7±1.3	13.4±1.5	3.3±0.02
Ti-1 mm	SGL	AEM	CCS	35.8±3.5	13.5±1.5	4.5±0.05
Ti-0.15 mm	SGL	AEM	CCS	38.4±4.2	10.7±1.2	5.5±0.05
SSM	SGL	AEM	CCM	48.5±2.7	11.6±2.8	6.2±0.08
H23	SGL	AEM	CCM	40.6±5.3	9.7±0.9	3.5±0.002
Ti-1 mm	H23	CEM	CCM	6.5±0.3	0.65±0.4	2.8±0.05
Ti-0.15 mm	H23	CEM	CCM	27.2±4.8	5.2±2.2	3.2±0.15
Ti-1 mm	SGL	CEM	CCM	22.3±3.2	4.8±1.5	5.6±0.1
Ti-0.15 mm	SGL	CEM	CCM	21.9±3.1	4.2±0.3	5.0±0.4
SSM	SGL	CEM	CCM	28.9±2.3	5.6±0.8	3.10±0.007
H23	SGL	CEM	CCM	35.6±5.2	4.9±0.7	3.5±0.2
Ti-1 mm	H23	CEM	CCS	17.2±2.1	1.8±2.1	2.8±0.06
Ti-0.15 mm	H23	CEM	CCS	23.8±2.8	2.2±2.8	2.9±0.01
Ti-1 mm	SGL	CEM	CCS	31.1±5.9	8.9±5.1	5.5±0.1
Ti-0.15 mm	SGL	CEM	CCS	24.9±3.1	4.3±1.1	4.9±0.4
SSM	SGL	CEM	CCM	13.2±3.8	5.1±1.1	3.8±0.04
H23	SGL	CEM	CCM	27.8±2.6	7.3±1.3	3.8±0.003

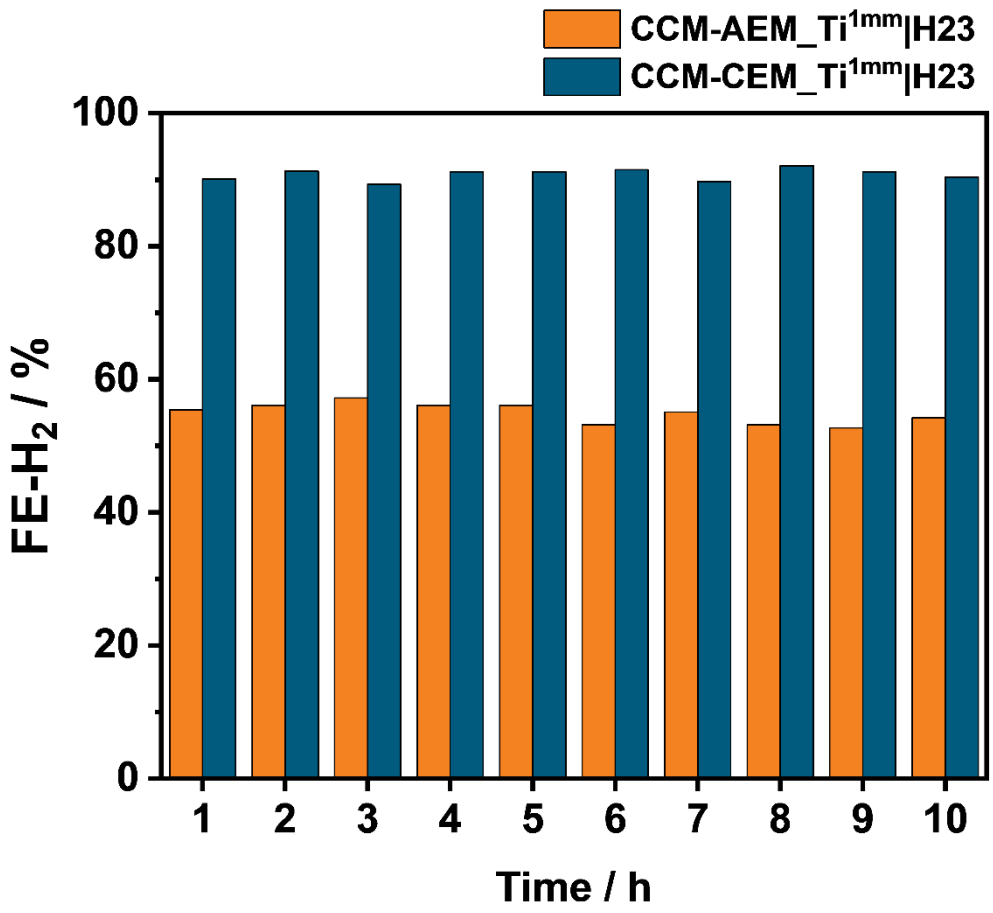

Figure S1. Faradaic Efficiency towards the generation of hydrogen for CCM-CEM_Ti^{1mm}|H23 and CCM-AEM_Ti^{1mm}|H23 at 80 mA cm^{-2} (Catholyte: 1 M MBY, 0.3 M KOH in H_2O, Anolyte: H_2O).

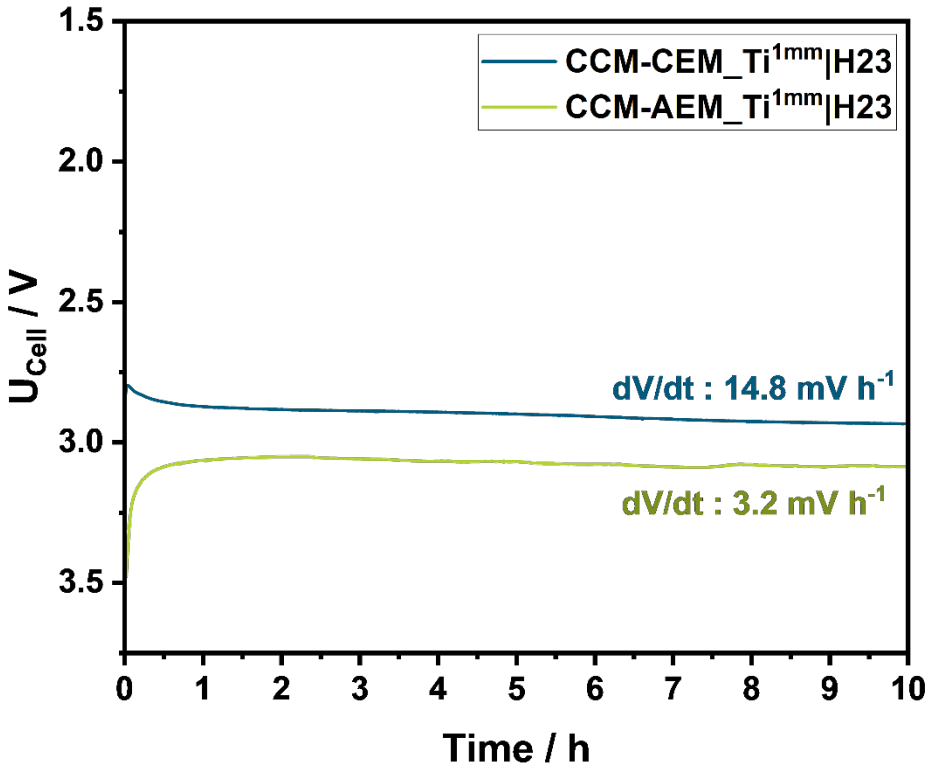

Figure S2. Cell voltage curves obtained during long-term experiments at 80 mA cm^{-2} for CCM-CEM_Ti^{1mm}|H23 and CCM-AEM_Ti^{1mm}|H23 (Catholyte: 1 M MBY, 0.3 M KOH in H_2O, Anolyte: H_2O – Electrolyte volumes were increased to 500 mL to better match the long-term conditions). The corresponsing voltage decay values over 10 h of electrolysis are also given.

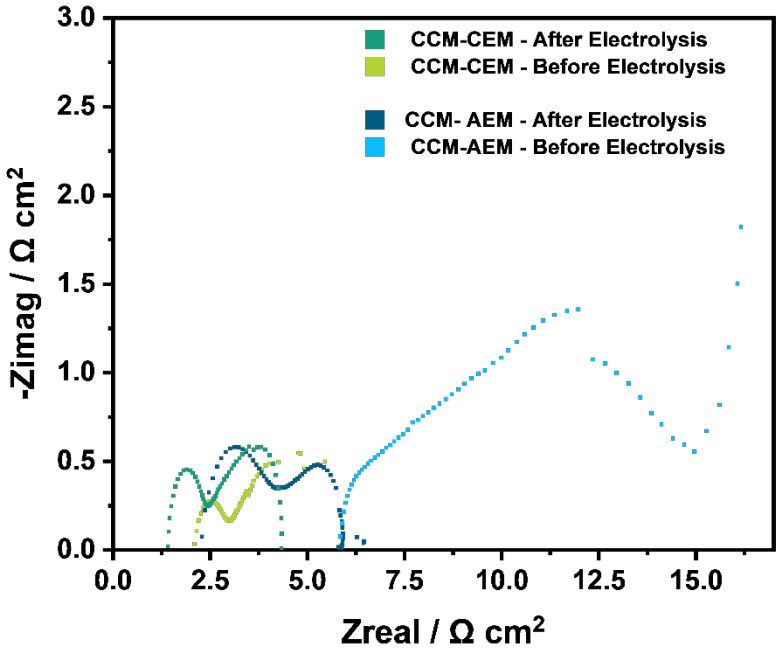

Figure S3. Impedance spectra for CCM-CEM_Ti^{1mm}|H23 and CCM-AEM_Ti^{1mm}|H23 2 (Catholyte: 1 M MBY, 0.3 M KOH in H_2O, Anolyte: H_2O) obtained before and after electrolysis at 80 mA cm^{-2} for 10 h. A previously employed EIS model used by Atobe and co-workers was employed to fit the obtained data.

AFM Results

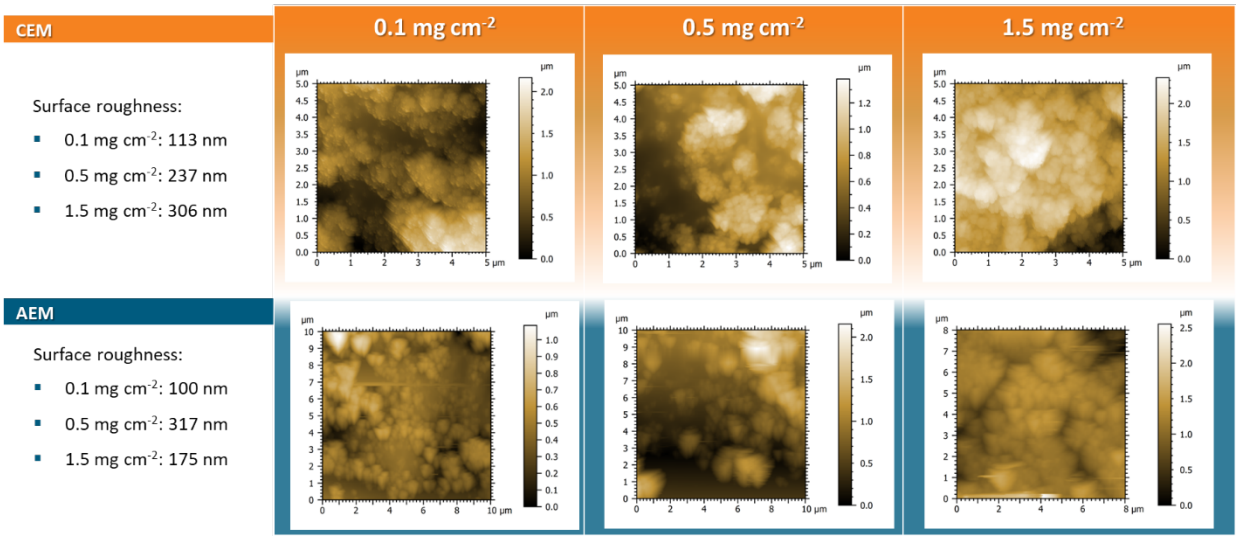

Figure S4. Results of the AFM analysis for the investigated CCM, CEM and AEM membranes with different loadings of IrO_2 as indicated in the upper row.

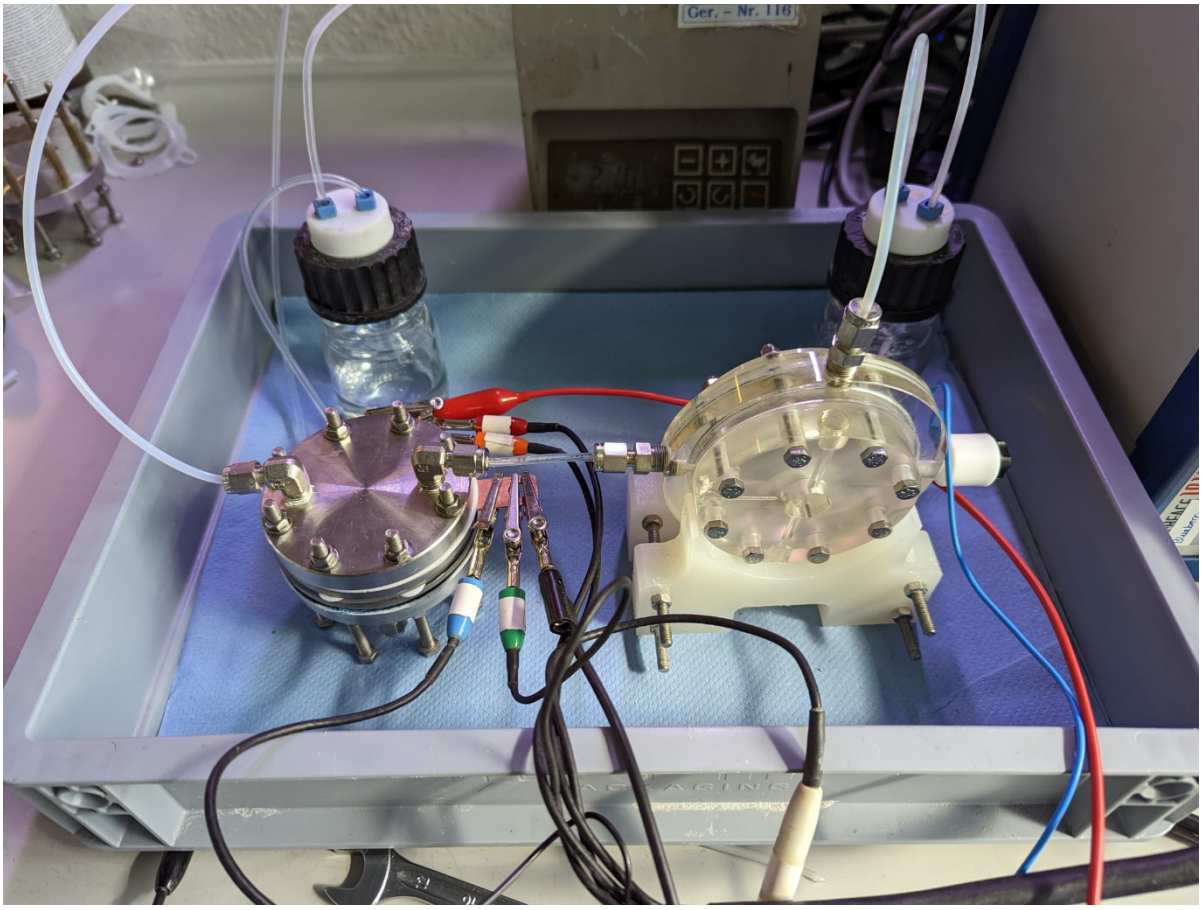

Figure S5. Photograph of the herein developed electrolyzer set-up to measure half-cell potentials during ECH in zero-gap electrolyzers.

Table S2. Analysis of the Ru resistances recorded at the half-cell and full-cell level during the investigation of the half-cell potentials for the ECH.

Cell assembly	U_{cell} / V	Ru^{Cell} / Ω	Associated voltage loss / V	$E^{Cathode}$ / V	Remaining Voltage / V
$_{CCM\text{-}AEM}Ti^{1}$|SGL	3.18	1.64	1.64	0.42	1.12
$_{CCS\text{-}AEM}Ti^{1}$|SGL	4.47	0.78	0.78	0.28	3.41
$_{CCM\text{-}AEM}Ti^{0.15}$|SGL	3.24	1.08	1.08	0.79	1.37
$_{CCS\text{-}AEM}Ti^{0.15}$|SGL	5.46	1.76	1.76	0.67	3.03
$_{CCM\text{-}CEM}Ti^{1}$|H23	2.79	0.72	0.72	0.51	1.56
$_{CCS\text{-}CEM}Ti^{1}$|H23	2.89	0.67	0.67	0.6	1.62
$_{CCM\text{-}CEM}Ti^{0.15}$|H23	3.28	0.59	0.59	0.45	2.24
$_{CCS\text{-}CEM}Ti^{0.15}$|H23	2.94	0.61	0.61	0.4	1.93

Improvement of the anolyte environment

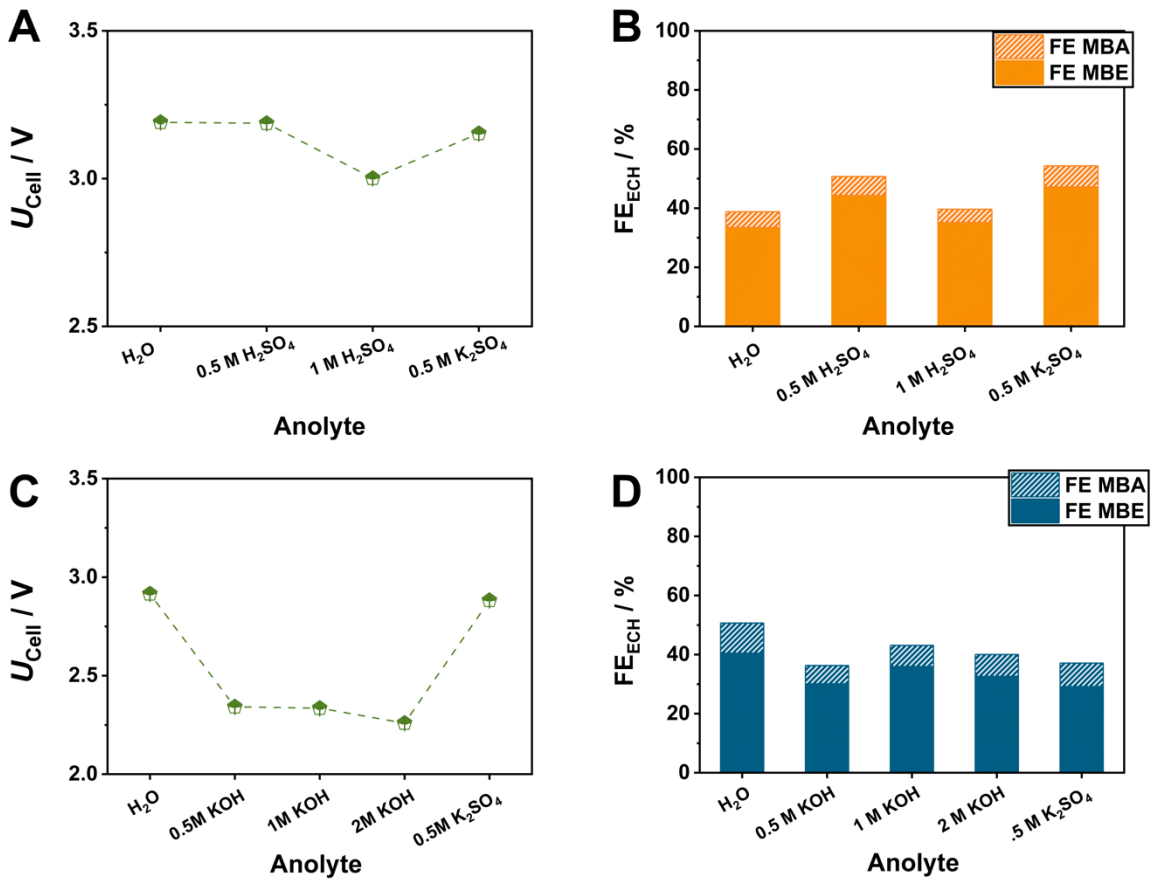

Figure S6. Effect of the anolyte on the electrochemical hydrogenation of MBY in CEM and AEM-separated zero-gap electrolyzers at 80 mA cm^{-2} after 1 h of electrolysis. For the investigation employing CEM, the CEM-CCM_Ti^{1mm}|SGL cell assembly was employed (A-B), while for the AEM, the AEM-CCM_$Ti^{0.15mm}$|H23 cell assembly was used (C-D).

Comparison of the obtained cell voltages and selectivities against the state-of-the-art

Table S3. Tabular comparison of different zero-gap and undivided reactor types for the electrochemical hydrogenation against the herein presented results. *Denotes the use of a hydrogen pump, ie hydrogen oxidation on Pt at the anode.

Cathode (Catalyst – PTL)	Anode (Catalyst-PTL)	Cathode Reaction	Anode Reaction	Membrane	FE_{ECH} / %	j / mA cm^{-2}	U_{cell} / V	Ref
Ag NPs on Carbon Cloth	NiFe	HMF Hydrogenation to BHMF	HMF Oxidation to FDCA (pH 13)	CEM	50	2	1.5	[3]
Ag NPs on Carbon Cloth	NiFe	HMF Hydrogenation to BHMF	HMF Oxidation to FDCA (pH 13)	AEM	50	2	1.5	[3]
Ag NPs on Carbon Cloth	NiFe	HMF Hydrogenation to BHMF	HMF Oxidation to FDCA (pH 13)	BPM	50	2	2.2	[3]
$Rh_{0.38}$/Pt/C	Pt/C on Carbon Paper	Neat Toluene Hydrogenation	Hydrogen Oxidation	CEM	ca. 100%	200	-0.02*	[4]
Pt/C on Carbon Paper	Pt/C on Carbon Paper	Neat Toluene Hydrogenation	Hydrogen Oxidation	CEM	ca. 85%	200	-0.04*	[4]
Pd on Carbon Cloth	Pt-mesh anode	1-Decene Hydrogenation	Water Oxidation (0.1 M H_2SO_4)	CEM	48	28	2.23	[5]
Pt on Carbon Cloth	Pt-mesh anode	1-Decene Hydrogenation	Water Oxidation (0.1 M H_2SO_4)	CEM	10	100	3.61	[5]
Bi Plate	Pt Plate	*cis,cis*.muconic acid hydrogenation	Water Oxidation (pH 7)	Undivided reactor	41	200	5.7	[6]
$Fe_3Ni_6S_8$ on H23	IrO_2 on Ti-0.15 mm	2-Methyl-3-butyn-2-ol hydrogenation	Water Oxidation (2M KOH)	AEM	49	80	2.9	**This work**
$Fe_3Ni_6S_8$ on H23	IrO_2 on Ti-0.15 mm	2-Methyl-3-butyn-2-ol hydrogenation	Water Oxidation (2M KOH)	AEM	49	80	2.2	**This work**
$Fe_3Ni_6S_8$ on H23	IrO_2 on Ti-0.15 mm	2-Methyl-3-butyn-2-ol hydrogenation	Water Oxidation (2M KOH)	AEM	49	80	2.9	**This work**

References

1 D. Tetzlaff, K. Pellumbi, D. M. Baier, L. Hoof, H. Shastry Barkur, M. Smialkowski, H. M. A. Amin, S. Grätz, D. Siegmund, L. Borchardt and U.-P. Apfel, *Chem. Sci.*, 2020, **11**, 12835.

2 K. Pellumbi, L. Wickert, J. T. Kleinhaus, J. Wolf, A. Leonard, D. Tetzlaff, R. Goy, J. A. Medlock, K. Junge Puring, R. Cao, D. Siegmund and U.-P. Apfel, *Chem. Sci.*, 2022, **13**, 12461.

3 H. Liu, T.-H. Lee, Y. Chen, E. W. Cochran and W. Li, *ChemElectroChem*, 2021, **8**, 2817.

4 T. Imada, M. Chiku, E. Higuchi and H. Inoue, *ACS Catal.*, 2020, **10**, 13718.

5 J. Benziger and J. Nehlsen, *Ind. Eng. Chem. Res.*, 2010, **49**, 11052.

6 M. N. Dell'Anna, M. Laureano, H. Bateni, J. E. Matthiesen, L. Zaza, M. P. Zembrzuski, T. J. Paskach and J.-P. Tessonnier, *Green Chem.*, 2021, **23**, 6456.